LINEARIZED FUN3D FOR RAPID AEROELASTIC DESIGN AND ANALYSIS

Shuchi Yang[1], P.C. Chen[1], and Zhicun Wang[1]

[1] ZONA Technology, Inc.
Scottsdale, Arizona
info@zonatech.com

Keywords: Aeroelasticity, Aeroservoelasticity, Linearized Euler solver, Generalized Aerodynamic Forces.

Abstract: A linearized unsteady Euler solver, referred to as ZONA Unstructured Linearized Unsteady Solver (ZULUS), is developed to solve the linearized frequency-domain Euler equation on an unstructured mesh using the steady background flow solution generated by the FUN3D Navier-Stokes (N-S) solver developed NASA Langley. ZULUS can generate an accurate unsteady aerodynamic solution in the small perturbation sense about a nonlinear steady flow condition with a transpiration boundary condition that is applied on the stationary mesh. It also can avoid the moving mesh problem associated with applying the exact N-S boundary condition which requires additional computational resources, and becomes very complex in dealing with the discontinuous displacement in mode shapes such as the control surface modes for which generating a computational mesh could be a very tedious effort. Using the generalized aerodynamic forces due to structural modes, control surface kinematic modes and gust excitation generated by ZULUS, one can design a flutter suppression and gust load alleviation controller using the modern control design schemes and perform aeroservoelastic analysis for the open-loop and closed-loop aeroelastic systems

1 BACKGROUND AND MOTIVATION

Flight-by-wire flight vehicles rely on flight control systems to achieve the desired stability and performance of the rigid body motion. Flight control systems for controlling the rigid body motion usually employ high gain feedback loop control systems that have become powerful enough to influence the aeroelastic response of the aircraft. In the flight-by-wire aircraft, the control system continuously receives the information of the aircraft motion from sensors and gives commands to the actuators to deflect the control surfaces for controlling the aircraft rigid body motion. However, some sensors capture both the rigid and elastic motions and may provide incorrect information to the control system if the effects of the elastic motions are not properly filtered out by the control law. As a result, the control surfaces may generate unwanted aerodynamic forces that can further amplify the aeroelastic response; rendering a self-excited instability. This type of instability due to the adverse coupling among structural dynamics, unsteady aerodynamics and control system is called aeroservoelastic (ASE) instability. Nowadays, ASE analysis for proving the under-designed flight-by-wire aircraft to be free from ASE instability is one of the Federal Aviation Administration (FAA) requirements for aircraft airworthiness certification.

Modern aircraft are being designed for optimal aerodynamic performance and can suffer from strong separated flow conditions when operated at off design conditions. In the design phase an accurate prediction of the aeroelastic effects/loads is important for design of the airframe structure and design of maneuver load/gust load alleviation systems. In the conceptual design stage the designer often requires a choice of whether to resolve the aeroelastic problems by active or passive means. For example, it is well known that the flying wing type of configuration is prone to body-freedom flutter (BFF) problem. Because of the low pitch inertia leading to higher frequency of the short-period mode, this short-period mode may couple with the elastic mode thus inducing the BFF phenomenon. Several configurations have encountered such a BFF problem, such as the B-2 aircraft and X-56A. Because increasing the BFF boundary by passive means requires a large weight penalty, a flutter suppression control system was incorporated in B-2 [1] whose controllability for flutter suppression has been demonstrated by flight test. Also, when carrying external stores, some fighter may encounter the limit cycle oscillation (LCO). For instance, the F/A-18 fighter is equipped with a flutter suppression control system called the active aeroelastic oscillation control to suppress the LCO due to the carriage of high pitch inertia stores on the outboard pylons of the wing [2].

The maneuver and gust loads on transport aircraft usually are two of the critical design loads that dominate the structural design. To avoid the weight penalty for reducing the dynamic loads, both Boeing 787 and Airbus A320 are equipped with a maneuver and gust load alleviation control law using the aileron and spoiler to provide the control authority. The design of an effective maneuver and gust load alleviation controller requires an enormous amount of wind tunnel testing and flight testing to tune the control laws. Thus, an accurate aeroservoelastic model based on the Navier-Stokes flow equations can greatly reduce wind tunnel and flight test time. These examples show the importance of the availability of a plant model to correlate the control input to the sensor output in the early design stages, which allows the designer to rapidly design a control system and to evaluate its performance for flutter suppression and gust load alleviation.

2 REVIEW OF THE CURRENT ASE METHODOLOGY USED BY THE INDUSTRY

Each The current aeroservoelastic (ASE) methodology used by the industry starts from the generation of the generalized aerodynamic forces (GAF) using linear potential unsteady aerodynamic methods. Three types of the GAF are required for generating a complete plant model: (i) GAF due to structural modes, (Q_{hh}), (ii) GAF due to the control surface kinematic modes (Q_{hc}), and (iii) GAF due to gust (Q_{hg}). Usually these GAFs are computed in the frequency domain ($i\omega$) by the linear potential unsteady aerodynamic methods. By applying the Rational Function Approximation (RFA) technique, these GAFs are transformed into state-space form and can be combined with the structural state-space equation, actuator state-space equation and the sensor state-space equation to form the state-space equation of the plant model in the following general form:

$$\begin{aligned} \{\dot{X}\} &= [A]\{X\} + [B]\{U\} + [B_g]\{\bar{w}_g\} \\ [y] &= [C]\{X\} + [D]\{U\} + [C_g]\{\bar{w}_g\} \end{aligned} \tag{1}$$

Where $\{X\}$ is the state vector containing the structural states, actuator states and the aerodynamic lags due to RFA, $[y]$ is the sensor output vector and $\{U\}$ and $\{\bar{w}_g\}$ are the control surface and gust input vectors, respectively. Because most modern control law design

schemes require the plant model in the state space form as a starting point, this plant model can be directly adopted by those modern control schemes for control law design. Or it can be connected to a rigid body flight dynamic model to perform an ASE analysis. Note that the eigenvalues of the system matrix [*A*] are the frequencies and damping of the aeroelastic system which can be used to evaluate the flutter boundary of the open-loop aeroelastic system.

However, the linear potential unsteady aerodynamic methods adopted by the current industrial ASE methodology are not valid for complex flows, such as the presence of a transonic shock, flow separation due to high angle of attack, etc. Therefore, it is highly desirable to develop a CFD-based reduced order model using a linearized flow solver that can rapidly generate the above-mentioned GAFs about a nonlinear steady Navier-Stokes (N-S) solution flow field. Once these GAFs are generated, the plant model can be developed using the similar steps as the current linear ASE methodology employed by the industry for control law design. One such N-S solver is FUN3D developed by NASA Langley.

3 FUN3D FLOW SOLVER DEVELOPED BY THE NASA LANGLEY RESEARCH CENTER

In FUN3D is a Navier-Stokes (N-S) solver [3] that uses unstructured mesh with the various turbulence modeling options for steady and unsteady aerodynamic simulations. The recent study by ZONA on an F-15 demonstrates the accuracy of FUN3D for steady aerodynamics prediction. Figure 1 presents the experimental data on the F-15 wing at M = 0.609 and a high angle of attack = 15.12°, which reveals the large flow separation, especially on the outboard section on the F-15 wing. This separated flow is accurately predicted by the FUN3D steady solution. The FUN3D solution using approximately 14 million unstructured grid points takes 20-30 hours of computational time at each flow condition with 32 processors. This clearly shows the computational accuracy and efficiency of the FUN3D for steady aerodynamic prediction.

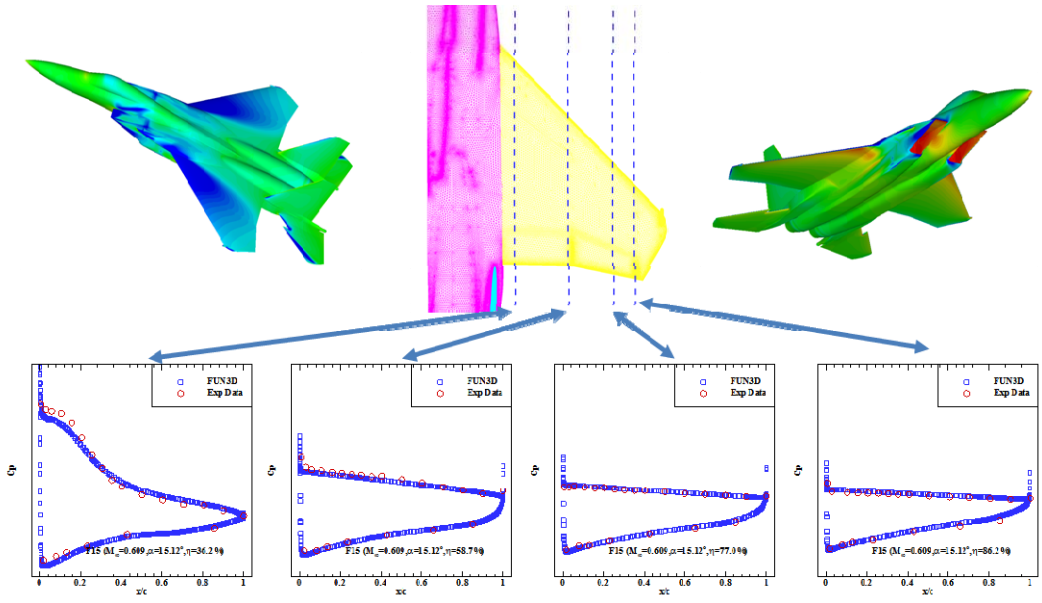

Figure 1. Comparison of the Pressure Distribution Between FUN3D Results with the Experimental Data on the F-15 at Mach = 0.609 and Angle of Attack = 15.12°

For aeroelastic computation using FUN3D unsteady aerodynamic capability, the FUN3D couples the time-accurate scheme for solving the N-S equation with the structural equations to compute the aeroelastic responses. Three technical issues are involved in this approach.

(1) The computational time for the unsteady aerodynamic cases is at least 1~2 orders higher than that of the steady aerodynamics cases. For complex configurations, this long computational time is not acceptable for routine industrial aeroelastic and ASE analysis.

(2) The computational mesh must be deformed according to the structural deformation using a moving mesh algorithm. This moving mesh algorithm requires additional computational resources, and becomes very complex in dealing with the discontinuous displacement in mode shapes such as the control surface modes for which generating a computational mesh could be a very tedious effort.

(3) The FUN3D unsteady aerodynamic capability does not lead to a state-space equation representing the plant model. Therefore, this unsteady aerodynamic capability of FUN3D cannot be directly adopted for the control law design.

4 ZONA EULER UNSTEADY SOLVER (ZEUS)

ZEUS [4] is an Euler unsteady solver with boundary layer coupling option. To generate the GAFs, Q_{hh}, Q_{hc} and Q_{hg}, ZEUS employs a linearized Euler solver [5] that solves the frequency-domain linearized Euler equation in conservative differential form and curvilinear coordinates, (ξ,η,ς), which reads:

$$i\omega\tilde{Q}(i\omega)+\frac{\partial\left(\bar{A}_{\xi}\tilde{Q}(i\omega)\right)}{\partial\xi}+\frac{\partial\left(\bar{A}_{\eta}\tilde{Q}(i\omega)\right)}{\partial\eta}+\frac{\partial\left(\bar{A}_{\varsigma}\tilde{Q}(i\omega)\right)}{\partial\varsigma}=0 \tag{2}$$

Where $\tilde{Q}(i\omega)$ is the vector of the unsteady perturbed conservative fluid variables and $\bar{A}_{\xi}$, $\bar{A}_{\eta}$, $\bar{A}_{\tau}$ are the mean flow convective flux Jacobians (called steady background flow) that are provided by the ZEUS steady Euler solver with boundary layer effects.

To solve the linearized Euler equation, ZEUS employs the transpiration boundary condition that can avoid the issues associated with the moving mesh algorithm altogether. The transpiration boundary condition is a first order Taylor's expansion of the exact Euler boundary condition on the instantaneous moving surface $S(x,y,z,t)=0$ about the non-moving stationary position of the surface $S_0(x, y, z) = 0$. The transpiration boundary condition of the linearized Euler equation reads:

$$\begin{aligned}\tilde{w}_n(x,y,z,t)\big|_{s_0} &= \tilde{u}(x,y,z,t)\big|_{s_0}\,\partial S_o/\partial x+\tilde{v}(x,y,z,t)\big|_{s_0}\,\partial S_o/\partial y\\ &\quad+\bar{u}(x,y,z)\tilde{\phi}_x(x,y,z,t)+\bar{v}(x,y,z)\tilde{\phi}_y(x,y,z,t)+\dot{\tilde{\phi}}(x,y,z,t)/V\end{aligned} \tag{3}$$

where $\tilde{w}_n(x,y,z,t)$, $\tilde{u}(x,y,z,t)$ and $\tilde{v}(x,y,z,t)$ are the unsteady perturbation velocity along the normal and tangential directions on the stationary surface mesh, $\bar{u}(x,y,z)$ and $\bar{v}(x,y,z)$ are the steady flow velocities along the tangential direction that are provided by the steady Euler equation and $\tilde{\phi}(x,y,z,t)$ is the structural mode shape or the control surface kinematic mode whose amplitude is assumed to be small and is used as the small parameter involved in the

Taylor's expansion to derive the transpiration boundary condition.

Assuming the response to be a simple harmonic motion; i.e. $\tilde{w}_n(x,y,z,t) = w_n(x,y,z,i\omega)e^{i\omega t}$, $\tilde{u}(x,y,z,t) = u(x,y,z,i\omega)e^{i\omega t}$, $\tilde{v}(x,y,z,t) = v(x,y,z,i\omega)e^{i\omega t}$, and $\tilde{\phi}(x,y,z,t) = \phi(x,y,z,i\omega)e^{i\omega t}$, Equation (4) can be transformed into the frequency domain:

$$w_n(x,y,z,i\omega)\big|_{S_0} = u(x,y,z,i\omega)\big|_{S_0}\,\partial S_o/\partial x + v(x,y,z,i\omega)\big|_{S_0}\,\partial S_o/\partial y + \bar{u}(x,y,z)\phi_x(x,y,z,i\omega) + \bar{v}(x,y,z)\phi_y(x,y,z,i\omega) + i\omega\phi(x,y,z,i\omega)/V \tag{4}$$

Because all terms involved in Equation (4) are evaluated on the stationary surface mesh, $S_0(x,y,z) = 0$, no moving mesh is required for the transpiration boundary condition. Applying Equation (4) to the linearized frequency-domain Euler equation yields the frequency-domain unsteady pressures and GAFs due to structural mode shapes and control surface kinematic modes.

Incorporating the gust excitation into the transpiration boundary condition is very straightforward. The time-domain gust excitation for generating the elementary gust solution is a traveling Dirac delta function, $\delta(t\text{-}(x\text{-}x_0)/V)$, where x_0 is the reference point of the gust, V the free stream velocity and x is a point on the surface mesh. The frequency-domain counterpart of the traveling Dirac function can be immediately obtained by Fourier transform:

$$\bar{\delta}(i\omega) = \int_{-\infty}^{\infty} \delta(t-(x-x_0)/V)e^{-i\omega t}dt = e^{-i\omega(x-x_0)/V} \tag{5}$$

The induced angle of attack due to the frequency-domain traveling Dirac delta function can be directly plugged into the transpiration boundary condition to yield the gust solution such as:

$$w_n(x,y,z,i\omega)\big|_{S_0} = u(x,y,z,i\omega)\big|_{S_0}\,\partial S_o/\partial x + v(x,y,z,i\omega)\big|_{S_0}\,\partial S_o/\partial y - \bar{u}(x,y,z)e^{-i\omega(x-x_0)/V} \tag{6}$$

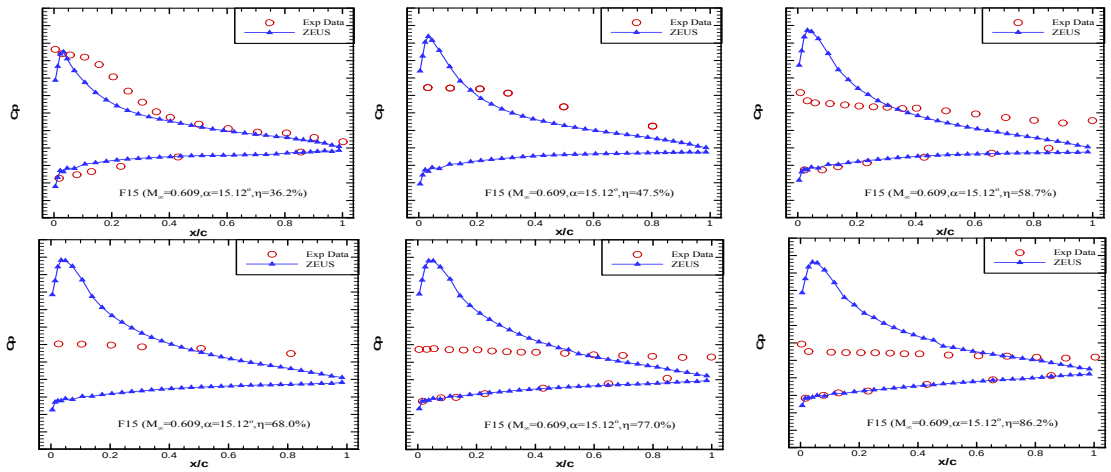

Figure 2. Comparison of the Pressure Distribution between ZEUS Result and the Experimental Data on the F-15 at Mach = 0.609 and AoA = 15.12°

However, the boundary layer method incorporated in ZEUS is a two dimensional Green's lag entrainment integral boundary-layer method [6] which is known to be incapable of handling large flow separation. To show this, the steady pressure distribution on the F-15 at

Mach=0.609 and angle of attack=15.12 degrees previously shown in Figure 1 is re-investigated using the ZEUS steady Euler solver and is presented in Figure 2. It can be seen that, unlike the FUN3D N-S solver that can capture the large flow separation very well, the ZEUS steady Euler solver with the Green's lag entrainment integral boundary-layer method is totally incapable of handling such a complex flow problem. Since the accuracy of the unsteady flow solution obtained from a lower fidelity linearized flow solver depends on the accuracy of the steady flow solution. Therefore, one can conclude that the accuracy of the ZEUS linearized unsteady Euler solution at high angle-of-attack condition is unacceptable.

5 FORMULATION OF LINEARIZED EULER SOLVER USING STEADY BACKGROUND FLOW COMPUTED BY FUN3D

The full Navier-Stokes (N-S) equation in curvilinear coordinates can be represented by the following equation:

$$\partial Q/\partial t + \partial H_1/\partial \xi + \partial H_2/\partial \eta + \partial H_3/\partial \varsigma = \partial H_{v1}/\partial \xi + \partial H_{v2}/\partial \eta + \partial H_{v3}/\partial \varsigma \tag{7}$$

where Q is the vector of conservative fluid variables, H_1, H_2, and H_3 are the convective flues in three curvilinear coordinate directions.

The right hand terms of Equation (7) represent the viscous terms and the left hand terms represent the unsteady variation and convection terms.

With the same idea as the linearized Euler solver in ZEUS, the total unsteady terms can be divided into to a steady part ($\bar{Q}$, $\bar{H}_i$, and $\bar{H}_{v_i}$) and an unsteady small perturbation part ($\tilde{Q}(t)$, $\tilde{H}_i(t)$ and $\tilde{H}_{v_i}(t)$);

$$Q = \bar{Q} + \tilde{Q}(t),\ H_i = \bar{H}_i + \tilde{H}_i(t),\ H_{v_i} = \bar{H}_{v_i} + \tilde{H}_{v_i}(t),\quad i = 1,2,3$$

Substituting the above equations into Equation (7), we can get two sets of equations. The first is the steady part shown as follows:

$$\partial \bar{H}_1/\partial \xi + \partial \bar{H}_2/\partial \eta + \partial \bar{H}_3/\partial \varsigma = \partial \bar{H}_{v1}/\partial \xi + \partial \bar{H}_{v2}/\partial \eta + \partial \bar{H}_{v3}/\partial \varsigma \tag{8}$$

Equation (8) has the same form as Equation (8) except that the time derivative term is absent. Therefore, Equation (8) can be solved by the pseudo time marching scheme of FUN3D N-S solver.

The second set of equations is the linearized Navier-Stokes equation which reads:

$$\frac{\partial(\tilde{Q}(t))}{\partial t} + \frac{\partial(\bar{A}_\xi \tilde{Q}(t))}{\partial \xi} + \frac{\partial(\bar{A}_\eta \tilde{Q}(t))}{\partial \eta} + \frac{\partial(\bar{A}_\varsigma \tilde{Q}(t))}{\partial \varsigma} = \frac{\partial(\bar{B}_\xi \tilde{Q}(t))}{\partial \xi} + \frac{\partial(\bar{B}_\eta \tilde{Q}(t))}{\partial \eta} + \frac{\partial(\bar{B}_\varsigma \tilde{Q}(t))}{\partial \varsigma} \tag{9}$$

Where $\bar{B}_\xi$, $\bar{B}_\eta$, $\bar{B}_\tau$ are the mean viscous flux Jacobians. These Jacobians only includes the steady variables and are defined herein as the steady background flow. Applying Fourier transform, the frequency-domain counterpart of Equation (9) reads:

$$i\omega\tilde{Q}(i\omega) + \frac{\partial(\bar{A}_\xi \tilde{Q}(i\omega))}{\partial \xi} + \frac{\partial(\bar{A}_\eta \tilde{Q}(i\omega))}{\partial \eta} + \frac{\partial(\bar{A}_\varsigma \tilde{Q}(i\omega))}{\partial \varsigma} = \frac{\partial(\bar{B}_\xi \tilde{Q}(i\omega))}{\partial \xi} + \frac{\partial(\bar{B}_\eta \tilde{Q}(i\omega))}{\partial \eta} + \frac{\partial(\bar{B}_\varsigma \tilde{Q}(i\omega))}{\partial \varsigma} \tag{10}$$

Equation (10) is the linearized frequency-domain N-S equation that can generate the frequency-domain GAFs. However, directly solving Equation (10) for aeroelastic and aeroservoelastic applications may have the following technical issues:

(1) Solving Equation (10) requires the viscous mesh, which needs to be much more refined than the inviscid mesh. This lead to an increased computational time when compared to the linearized Euler solver.

(2) Since deriving the transpiration boundary condition for the N-S equation is very difficult and currently not available, in order to solve Equation (10) the moving mesh algorithm is required. Thus, the technical issues associated with the moving mesh algorithm for solving the linearized N-S equation are the same as for solving the full unsteady N-S equation.

To circumvent the above technical issues, we developed a hybrid approach, referred herein to as ZONA Unstructured Linearized Unsteady Solver (ZULUS), that solves the linearized Euler equation by ignoring the terms on the right hand side of Equation (10), but uses the steady background flow from the steady N-S equation of FUN3D. In so doing, the transpiration boundary condition of ZEUS can be directly adopted by ZULUS to avoid the moving mesh issues.

6 VALIDATION OF ZULUS WITH TDT MEASURED UNSTEADY PRESSURES ON THE BACT WING

The The Benchmark Active Controls Technology (BACT) [7] wing is a rectangular wing with an NACA0012 airfoil section that was mounted on the Pitch and Plunge Apparatus (PAPA) and was tested in the NASA Langley Transonic Dynamic Tunnel (TDT). The BACT wing has a trailing edge (T.E.) control surface, an upper surface (U.S.) spoiler, and a lower surface (L.S.) spoiler. TDT measured unsteady pressures due to trailing edge control surface oscillation and spoiler oscillation at various Mach numbers (M), mean angles of attack (α), mean T.E. control surface deflection (δ_{teo}) and mean upper spoiler (δ_{uso}) as well as mean lower spoiler δ_{lso}) deflections are available. These unsteady pressure measurements are used to validate ZULUS for unsteady aerodynamic analysis and to demonstrate the effectiveness and accuracy of the transpiration boundary condition for modeling control surface and spoiler oscillations.

Validation with the Linear Unsteady Aerodynamic Method

Since the linear unsteady aerodynamic methods such as the Doublet Lattice Method [8] and ZONA6 [9] have been adopted by aerospace industry for many years as the primary tools for aeroelastic analysis, the industrial aeroelastic engineers usually demand that any CFD unsteady aerodynamic method be validated with the linear theory at linear flow regions before it is accepted as an industrial tool. This validation is accomplished by the good agreement between ZULUS and the linear theory (ZONA6) on the BACT wing due to the trailing edge flap oscillation at M=0.3 and reduced frequency (k)=0.108 and is shown in Figure 3. Two sets of unsteady pressure coefficients (C_p) are computed by ZULUS; the first is for the thickness ratio (t/c)=12% and the second for t/c=3%. It can be seen that when t/c is decreased, ZULUS solution approaches the linear theory that only can model the wing as a flat plate. This validation case also shows that the thickness effects do have impact on the unsteady pressures even at linear flow regions.

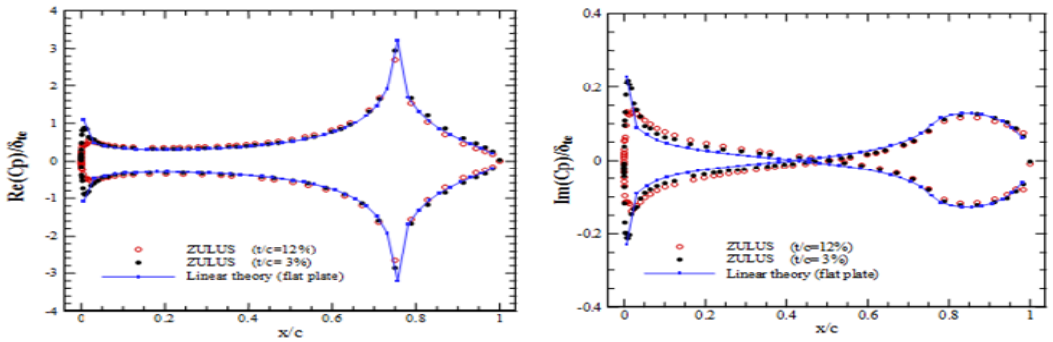

(a) Real Part **(b) Imaginary Part**

Figure 3 Unsteady C_p along 60% span on BACT Wing at M=0.3, α=0° due to Trailing Edge Oscillation at k=0.108

Imperfection of the BACT Wing Wind Tunnel Model

The BACT wing was tested in TDT with the heavy gas (R-12) to measure the steady and unsteady pressures. During the process of validating ZULUS with TDT data on the BACT wing, it was found that the BACT wing wind tunnel model has imperfection on its surface. Shown in Figure 4 is a small gap along the leading edge of the spoiler at 60% chord. The exact shape of the gap is unknown and is difficult to be modeled by the CFD mesh. This small gap creates discontinuities in both the measured steady pressure distribution at M=0.77 and mean trailing edge deflection angle (δ_{teo})=5^o and the measured unsteady pressure distribution due to trailing edge oscillation at k=0.108. These discontinuities are shown in Figure 5. Therefore, it is expected this small gap may introduce discrepancy in correlating ZULUS solution with the TDT test data.

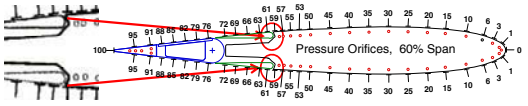

Figure 4 Imperfection on the BACT Wing Wind Tunnel Model

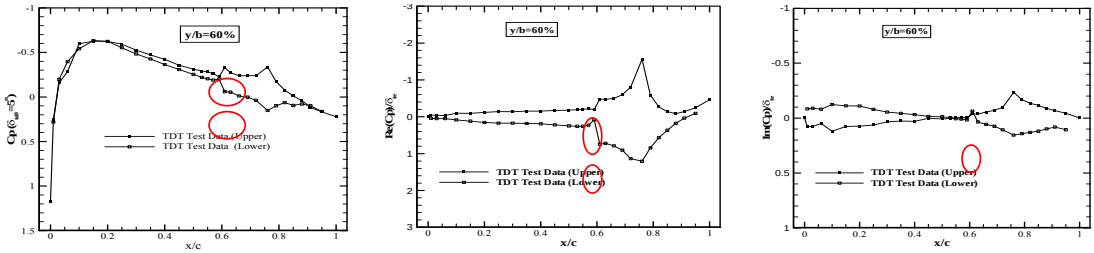

(a) Steady C_p **(b) Unsteady Re(C_p)** **(c) Unsteady Im(C_p)**

Figure 5 Discontinuities in C_p due to Imperfection on BACT Wing

Validation of Unsteady C_p at M=0.77, α=0^o and δ_{teo}= 0^o due to Trailing Edge Flap Oscillation

The steady and unsteady pressure was measured by TDT testing at M=0.77, α=0^o and mean trailing edge flap deflection angle (δ_{teo})= 0^o . Because ZULUS requires the FUN3D N-S flow solution as the steady background, FUN3D steady aerodynamic computation is first performed to compare its result to the TDT test data and that computed by ENS3DAE [10]. This comparison is shown in Figure 6. The TDT data shows that a weak transonic shock

occurs at approximately 25% chord. Both FUN3D and ENS3DAE slightly over-predict the transonic shock strength.

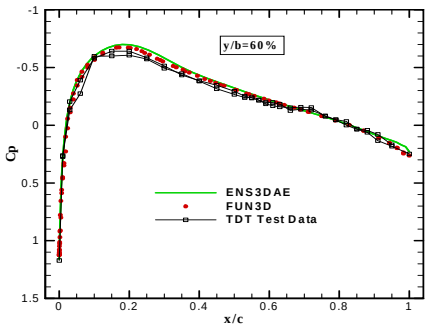

Figure 6 Steady C_p along y/b=60% on BACT Wing at M=0.77, $\alpha=0^o$ and $\delta_{te0}=0^o$

The FUN3D N-S solution is computed on an unstructured viscous mesh as the one shown in Figure 7(a). ZULUS uses an unstructured inviscid mesh that is much coarser than the viscous mesh. To map the steady background flow solution from the viscous mesh to the inviscid mesh, we developed a steady flow interpolation module in ZULUS. A typical mapped steady flow solution on the inviscid mesh of the BACT wing is shown in Figure 7(b).

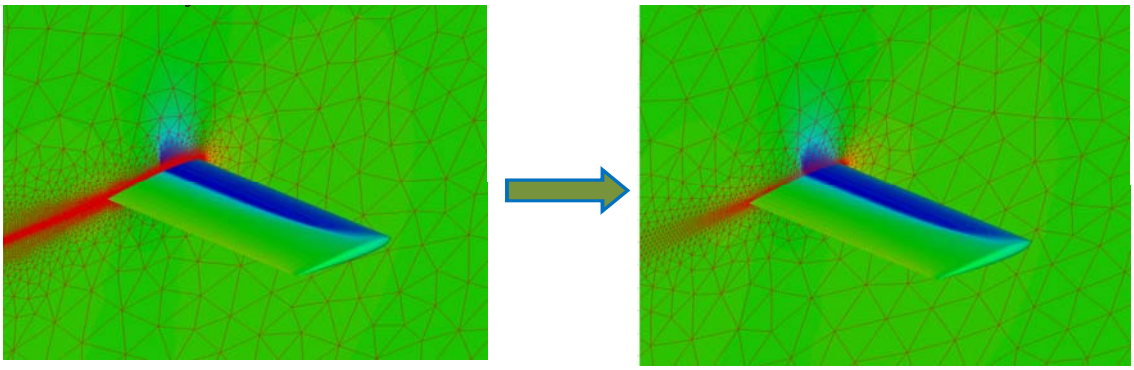

(a)Flow Solution by FUN3D on Viscous Mesh **(b) Interpolated Flow Solution on Inviscid Mesh**

Figure 7 Interpolation of FUN3D Steady Flow Solution from Viscous Mesh to Inviscid Mesh

The unsteady pressure was measured by oscillating the trailing edge flap at k=0.0542. Four sets of unsteady C_p along the 60% span on the BACT wing are presented in Figure 8; ZULUS result (shown by red circles), the TDT test data (shown by black squares), the ENS3DAE result (shown by solid green lines) and the CFL3D [10] result (shown by solid blue lines). Note that the ENS3DAE and CFL3D results are obtained by applying the Fourier transform to their time-accurate unsteady solutions.

At the 25% chord where the steady transonic shock occurs, all three CFD codes over-predict the unsteady shock strength. Because the unsteady shock strength and location are dominated by the steady shock strength and location in the small perturbation sense, the over-prediction of the steady shock strength by FUN3D, ENDS3DAE and CFL3D shown in Figure 6 leads to the over-prediction of the unsteady shock strength when compared to the TDT test data. On the trailing edge flap, the imaginary part of the unsteady C_p predicted by all three CFD codes are lower than that of the TDT test data. This discrepancy is probably due to the imperfection of the BACT wing wind tunnel model. Among the three CFD results, ZULUS agrees well with the ENS3DAE.

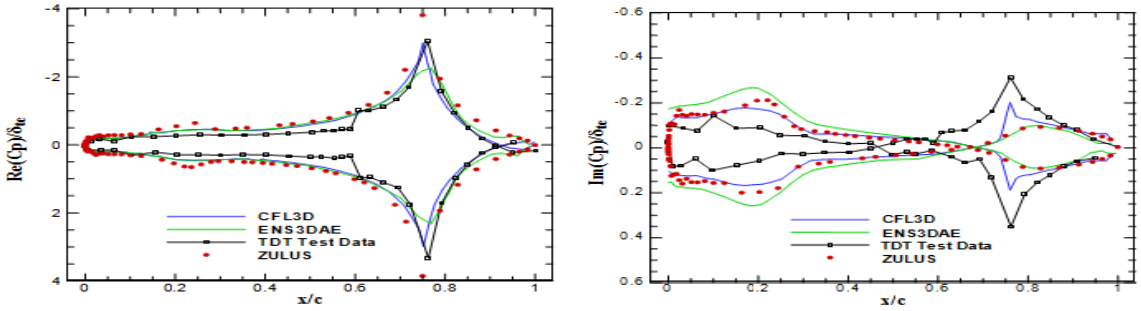

(a) Unsteady Re(C_p) **(b) Unsteady Im(C_p)**

Figure 8 Unsteady C_p along 60% span on BACT Wing due to Trailing Edge Flap Oscillation at k=0.0542 at M=0.77, **$\alpha=0^o$ and $\delta_{te0}=0^o$**

In order to investigate the impact of steady background flow on ZULUS unsteady results, we attempted to match the FUN3D steady C_p with the TDT data by varying the Mach number. Once a better agreement in the steady flow is achieved, this steady flow solution is used as the steady background flow for ZULUS to improve the unsteady prediction.

Shown in Figure 9 are the FUN3D steady C_p at M=0.77 and 0.75 in which the FUN3D result at M=0.75 agrees better with the TDT data measured at M=0.77 than the FUN3D results at M=0.77. Using the FUN3D solution at M=0.75 as the steady background flow, the unsteady shock strength at 25% chord predicted by ZULUS shown in Figure 10 is reduced and agrees better with the TDT data than ZULUS result using the FUN3D steady flow solution at M=0.77. This investigation verifies that the unsteady shock strength and location are dominated by the steady shock strength and location in the small perturbation sense.

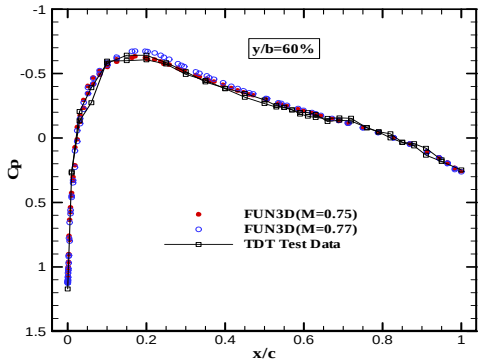

Figure 9 FUN3D Steady C_p on BACT Wing at **$\alpha=0^o$, $\delta_{te0}=0^o$ and M=0.77 as well as at M= 0.75**

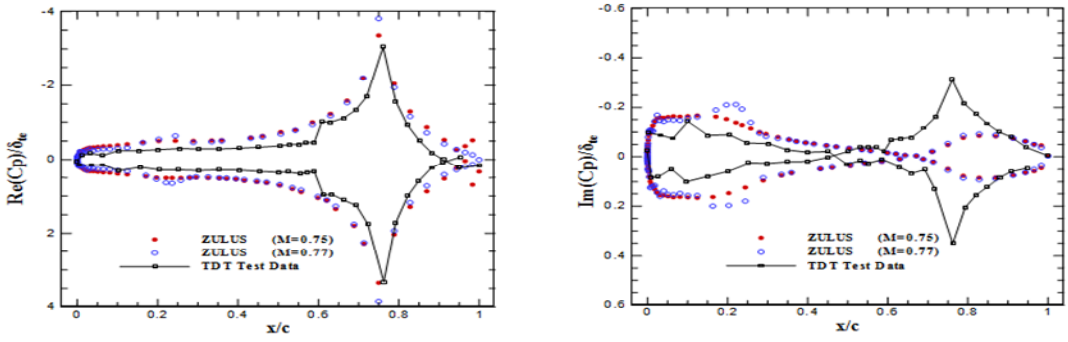

(a) Unsteady Re(C_p) **(b) Unsteady Im(C_p)**

Figure 10 ZULUS Unsteady C_p due to Trailing Edge Flap Oscillation at **$\alpha=0^o$**, **$\delta_{te0}=0^o$** and M=0.77 as well as at M=0.75

Validation of Unsteady C_p at M=0.77 $\alpha=4^o$ and $\delta_{teo}= 0^o$ due to Trailing Edge Flap Oscillation This case is identical to the case presented in Figures 9 and 10 except that the angle of attack is increased from 0^o to 4^o. Shown in Figure 11 is the TDT measured steady C_p at M=0.77 and $\alpha=4^o$ along with two sets of FUN3D computed steady C_p; one at M=0.77 and the other at M=0.75. Again, the FUN3D result at M=0.75 agrees better with the TDT data measured at M=0.77 than the FUN3D results at M=0.77. Bases on these two sets of FUN3D steady flow solutions, two sets of ZULUS unsteady C_p due to the trailing edge flap oscillation at k=0.108 along with the TDT test data at M=0.77 are presented in Figure 12. ZULUS result at M=0.75 agrees with the TDT data much better than ZULUS result at M=0.77; once again showing that the accuracy of the unsteady prediction highly depends on the accuracy of the steady flow solution.

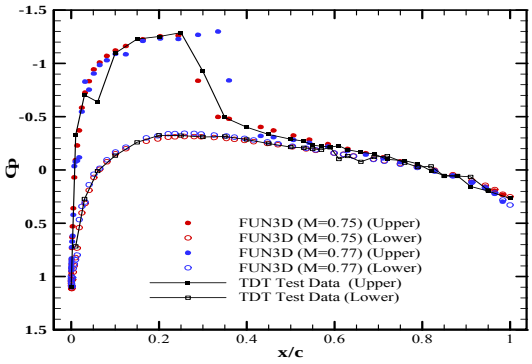

Figure 11 FUN3D Steady C_p on BACT Wing at **$\alpha=4^o$, $\delta_{te0}=0^o$ and M=0.77 as well as at M= 0.75**

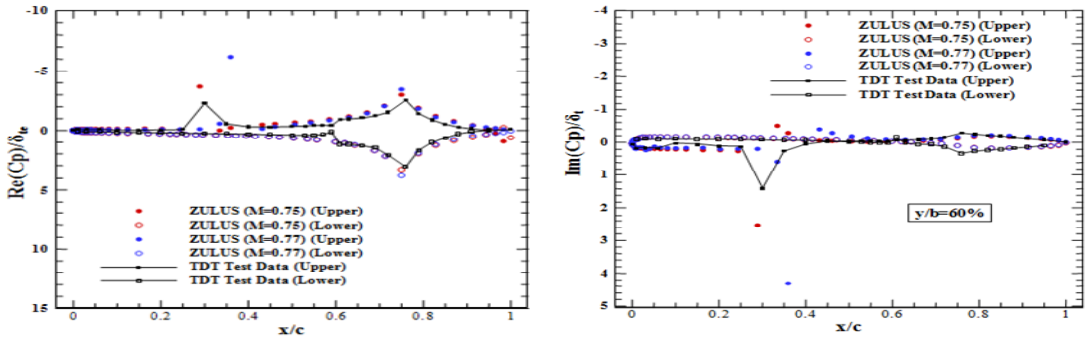

(a) Unsteady Re(C_p) **(b) Unsteady Im(C_p)**

Figure 12 ZULUS Unsteady C_p due to Trailing Edge Flap Oscillation at $\alpha=4^o$, $\delta_{te0}=0^o$ and M=0.77 as well as at M=0.75

Steady Flow Reconstruction for Steady Flow Solution at Mean Trailing Edge Flap Deflection Angle=5^o.

Because a wing with a mean control surface deflection represents a discontinuous surface, generation of a CFD mesh to model such a surface requires a tedious grid generation effort. However, using ZULUS linearized Euler solution at k=0, the steady flow solution to account for the control surface deflection effects can be obtained by a steady flow reconstruction procedure without regenerating a new mesh. The accuracy of this steady flow reconstruction procedure is demonstrated on the BACT wing with mean trailing edge deflection angle (δ_{teo})= 5^o. First, the steady C_p at $\delta_{teo}= 0^o$, denoted as $C_p(\delta_{teo}= 0^o)$, is obtained by the FUN3D steady N-S solver. Next, the real part of the unsteady solution at k=0 due to the trailing edge flap kinematic mode, denoted as Re[C_p(k= 0)], is computed by ZULUS. Such a trailing edge flap kinematic mode is shown in Figure 13. It should be noticed that this trailing edge flap kinematic mode is applied on the transpiration boundary condition of ZULUS; thereby

regeneration of a new mesh is not required. Finally, the steady C_p at $\delta_{teo}= 5^o$, denoted as $C_p(\delta_{teo}= 5^o)$, can be obtained immediately by substituting $\delta_{teo}=5^o$ into the following equation:

$$C_p(\delta_{te0} = 5°) = C_p(\delta_{te0} = 0°) + \delta_{te0} \Re[C_p(k = 0)] \tag{11}$$

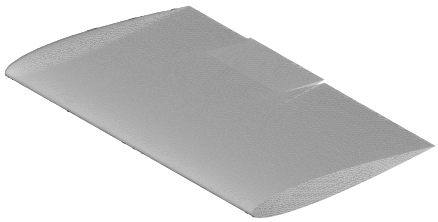

Figure 13 Trailing Edge Flap Kinematic Mode for the Transpiration Boundary Condition of ZULUS

In fact, the steady C_p at any δ_{teo} can be obtained by equation (11) as long as $\text{Re}[C_p(k= 0)]$ remains invariant with respect to δ_{teo}; i.e. the steady flow is linearly varying with respect to δ_{teo} which implies that δ_{teo} cannot be too large. The steady C_p obtained by the steady flow reconstruction procedure is referred herein to as FUN3D+ZULUS.

Figure 14 presents the steady C_p on the BACT wing with $\delta_{teo} =5^o$ at M=0.77 which includes four sets of results; the FUN3D+ZULUS result, the TDT test data, the ENS3DAE result and the CFL3D result. To reduce the grid generation effort, Bartels and Schuster [10] generated a "blended" mesh as the one shown in Figure 15 to approximate the discontinuous surface due to flap deflection and computed the steady flow solution using ENS3DAE and CFL3D. Using the steady flow reconstruction procedure, the FUN3D+ZULUS result is obtained on the mesh without a physically deflected flap. Good agreement between the FUN3D+ZULUS result and the ENS3DAE and CFL3D results as well as the TDT test data can be observed; validating the steady flow reconstruction procedure for steady flow solution with mean control surface deflection effects.

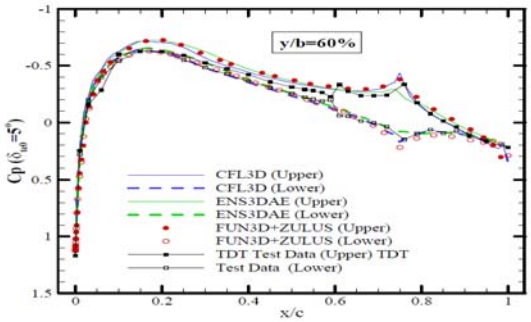

Figure 14 Steady C_p along y/b=60% on BACT Wing at M=0.77, $\boldsymbol{\alpha=0^o}$ **and** $\boldsymbol{\delta_{te0}=5^o}$

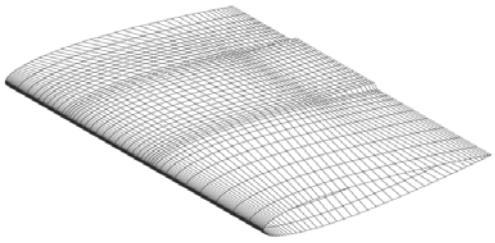

Figure 15 Blended Mesh to Account for Flap Deflection for ENS3DAE and CFL3D Computation

Unsteady C_p on BACT Wing at $\delta_{teo}=5^o$ due to Trailing Edge Flap Oscillation

The steady flow reconstruction procedure also can generate the conservative flow variables with mean control surface deflection effect using the following equation:

$$Q(\delta_{te0}) = Q(\delta_{te0} = 0°) + \delta_{te0}\,\mathrm{Re}[Q(k=0)] \tag{12}$$

Where $Q(\delta_{te0})$ denotes the conservative flow variables at a given δ_{te0}, $Q(\delta_{te0}=0°)$ denotes the conservative flow variables computed by FUN3D N-S solver at $\delta_{te0}=0^o$ and Re[$Q(k=0)$] denotes the unsteady conservative flow variables computed by ZULUS at $k=0$ using the control surface kinematic mode.

Now, $Q(\delta_{te0})$ can be served as the steady background flow with the control surface deflection effects for ZULUS to compute the unsteady aerodynamics. Figure 16 presents the comparison of the unsteady C_p on the BACT wing at M=0.77 and $\delta_{te0}=5^o$ due to the trailing edge flap oscillation at $k=0.108$ between ZULUS result using the steady background flow solution obtained by the flow reconstruction procedure and the TDT test data. The good correlation between these two results validates the steady flow reconstruction procedure to generate the steady background flow solution with control surface deflection effects for ZULUS unsteady computation, but without regenerating a mesh with a physically deflected control surface.

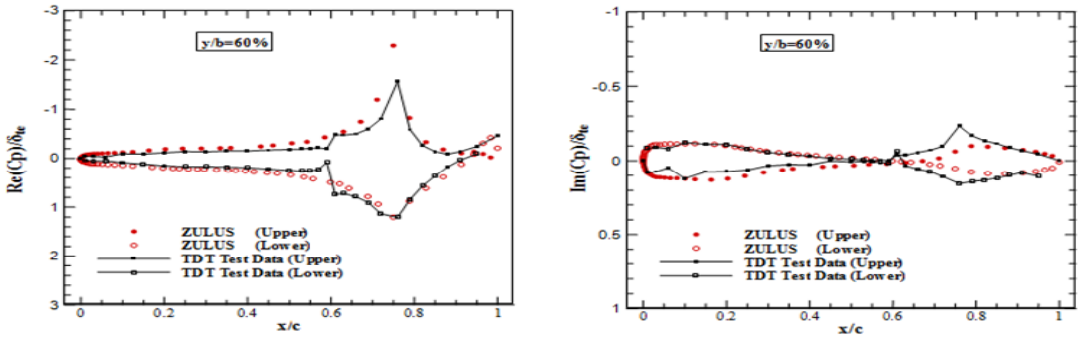

(a) Unsteady Re(C_p) **(b) Unsteady Im(C_p)**

Figure 16 Unsteady C_p along 60% span on BACT Wing due to Trailing Edge Flap Oscillation at k=0.108, M=0.77, $\boldsymbol{\alpha}=0^o$ and $\boldsymbol{\delta}_{te0}=5^o$

Steady Flow Reconstruction for Steady Flow Solution at Mean Upper Spoiler Deflection Angle=5^o

Using the steady flow reconstruction procedure, the steady C_p with mean upper spoiler deflection angle (δ_{us0}) can be obtained without generating a mesh with a physically deflected spoiler. The Re[$C_p(k=0$] is first computed by ZULUS with the upper spoiler kinematic mode such as the one shown in Figure 17 that is applied to the transpiration boundary condition. Then, the steady C_p at $\delta_{us0}=5^o$ can be immediately obtained by substituting $\delta_{uso}=5^o$ into the following equation:

$$C_p(\delta_{us0} = 5°) = C_p(\delta_{us0} = 0°) + \delta_{us0}\,\mathrm{Re}[C_p(k=0)] \tag{13}$$

Where $C_p(\delta_{us0}=0^o)$ is the FUN3D N-S solution at $\delta_{us0}=0^o$.

Good agreement of the steady C_p at M=0.77 and $\delta_{us0}=5^o$ between the results obtained by the steady flow reconstruction procedure and the TDT test data can be seen in Figure 18.

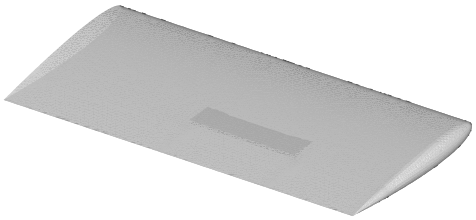

Figure 17 Upper Spoiler Kinematic Mode for the Transpiration Boundary Condition of ZULUS

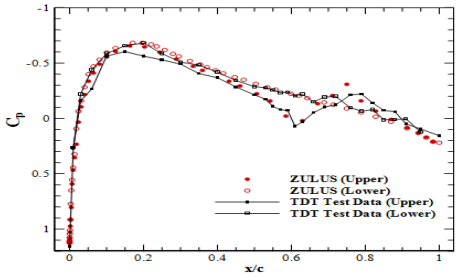

Figure 18 Steady Cp along y/b=60% on BACT Wing at M=0.77, □=0o and □us0=5o

Validation of Unsteady C_p at M=0.77 and δ_{us0}=5° due to Upper Spoiler Oscillation

The conservative flow variables at a mean upper spoiler deflection angle (δ_{us0})=5° also can be obtained using the steady flow reconstruction procedure by substituting δ_{us0}=5° into the following equation:

$$Q(\delta_{us0}) = Q(\delta_{us0} = 0°) + \delta_{us0} \square \mathrm{Re}[Q(k = 0)] \tag{14}$$

This conservative flow variables with δ_{us0}=5° effects serves as the steady back ground flow to compute the unsteady C_p due to upper spoiler oscillation at k=0.108 by ZULUS without regenerating a mesh to account for the mean spoiler deflection and spoiler oscillation. Three sets of unsteady C_p normalized by the oscillation amplitude of the upper spoiler (δ_{us}) are shown in Figure 19. The first two sets of results are the TDT test data with δ_{us}=2.37° and 4.47°. Large variation between these two sets of TDT test data can be seen, showing that the unsteady flow is highly nonlinear with respect to the mean spoiler deflection angle. The third result is ZULUS unsteady solution with steady background flow being provided by the steady flow reconstruction procedure. It can be seen that Re(C_p)/ δ_{us} computed by ZULUS agrees with the TDT test data reasonably well but $Im(C_p)$/ δ_{us} is significantly under-predicted. This discrepancy is probably coursed by the imperfection of the BACT wing wind tunnel model and the highly nonlinear flow structure due to spoiler deflection.

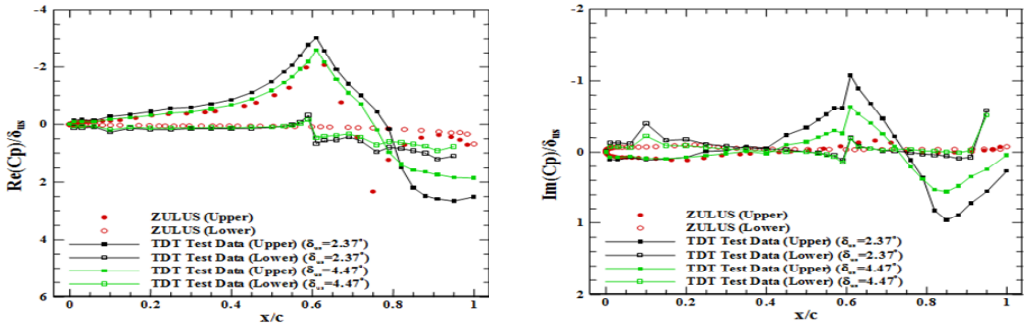

(a) Unsteady Re(C_p) **(b) Unsteady Im(C_p)**

Figure 19 Unsteady Cp along 60% span on BACT Wing due to Upper Spoiler Oscillation at k=0.108, M=0.77, □=0o and □us0=5o

7 VALIDATION OF ZULUS WITH TDT MEASURED FLUTTER BOUNDARY ON THE NACA 0012 BENCHMARK WING

Description of the NACA 0012 Benchmark Wing

The NACA 0012 Benchmark wing [11], referred to herein as B0012, has the identical external surface to the BACT wing but without the trailing edge flap and spoiler; thus without the imperfection on the surface. B0012 on the Pitch and Plunge Apparatus (PAPA) flexible mount system was tested in TDT using air (specific heat ratio=1.4) to measure its flutter boundary. B0012 on PAPA has only two degrees of freedom; namely the pitch mode and the plunge mode.

Because of the simple aerodynamic shape and simple structural properties, B0012 on PAPA is an ideal benchmark case to validate CFD codes for flutter boundary prediction.

Validation of ZULUS Predicted Flutter Boundary

Four sets of flutter boundaries of the B0012 on PAPA are presented in Figure 20. The first set is the TDT test data (shown by the black squares), the second set is the result computed by ZONA6 using the linear theory (shown by the dashed lines), the third set is result computed by ZEUS using its linearized Euler solver but using the steady background flow generated by the ZEUS' steady Euler solver (shown by the blue triangles). The forth set is the result computed by ZULUS using the FUN3D N-S solver generated steady background flow (shown by the red circles). The TDT test data shows that a transonic flutter pocket occurs at M=0.77 that is well captured by ZULUS. ZONA6 fails to capture this transonic flutter pocket because of its linear theory. ZEUS's linearized Euler solver can capture this transonic flutter pocket but over-predicts the flutter dynamic pressure. Note that all three flutter analyses are performed by the g-method flutter solution technique [12] except using their respectively generalized aerodynamic forces (Q_{hh}).

The excellent agreement of the flutter boundary between the TDT test data and ZULUS result is apparently due to the fact that ZULUS uses the high-fidelity steady flow solution provided by the FUN3D N-S solver as the steady background flow. On the other hand, the over-prediction of flutter dynamic pressure by the ZEUS' linearized Euler solver is apparently due to its low-fidelity steady flow solution generated by the steady Euler solver. This comparison, once again, demonstrates that if the steady background flow can be provided by a high fidelity code, the accuracy of the unsteady aerodynamics can be ensured even using a lower fidelity linearized flow solver.

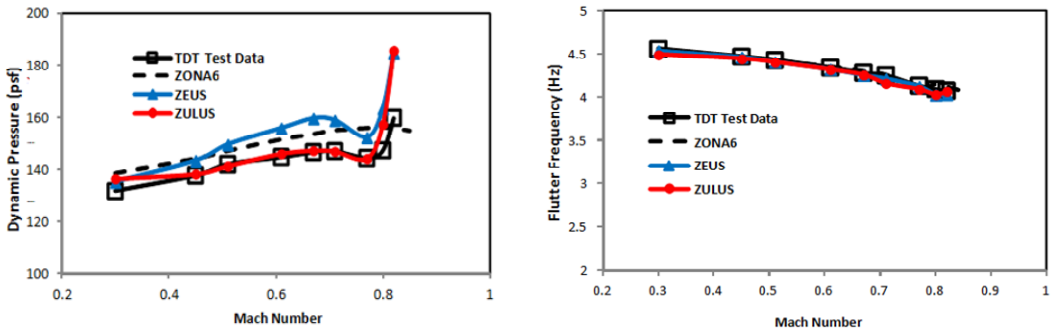

(a) Flutter Dynamic Pressure **(b) Flutter Frequency**

Figure 20 Flutter Boundary of B0012 on PAPA

8 CONCLUSIONS

In this work, an unstructured linearized Euler solver, called ZULUS, is developed that solves the frequency-domain linearized Euler equation based on the steady background flow solution provided by the FUN3D N-S solver. ZULUS can generate the frequency-domain generalized aerodynamic forces due to structural modes, control surface kinematic modes and gust excitation. These generalized aerodynamic forces can be directly plugged into the conventional frequency-domain flutter, ASE and gust analysis methodologies to generate flutter solution, ASE stability analysis and gust loads prediction.

Because of the transpiration boundary, ZULUS can avoid the moving mesh problem associated with applying the exact N-S boundary condition which requires additional computational resources, and becomes very complex in dealing with the discontinuous displacement in mode shapes such as the control surface modes for which generating a computational mesh could be a very tedious effort.

ZULUS has been validated with the TDT measured unsteady pressures on the BACT wing due to trailing edge control surface and spoiler oscillations which demonstrates that ZULUS can be effectively and efficiently used for aeroelastic and aeroservoelastic design and analysis.

9 REFERENCES AND CITATIONS

[1] Jacodson, S. B., Britt R. T., Freim, D. R. and Kelly, P. D. "Residual Pitch Oscillation (RPO) Flight Test Analysis on the B-2 Bomber", AIAA Paper, 1998-1805, 1998.

[2] Trame, L. W., Williams, L. E. and Yurkovich, R. N., "Active Aeroelastic Oscillation Control on the F/A-18 Aircraft." Presented at the AIAA Guidance Navigation and Control Conference. 19-21 August 1986. Snowmass, Colorado.

[3] Anderson, W. K., and Bonhaus, D. L.: “An Implicit Upwind Algorithm for Computing Turbulent Flows on Unstructured Grids”. Compt. and Fluids, Vol. 23, No. 1, pp. 1-21, 1994.

[4] Chen, P.C., Zhang, Z., Sengupta, A., and Liu, D. D., “Overset Euler/Boundary-Layer Solver with Panel-Based Aerodynamic Modeling for Aeroelastic Application,” Journal of Aircraft, Vol. 46, No. 6, November – December 2009.

[5] Zhichao Zhang , Shuchi Yang, P. C. Chen, "Linearized Euler Solver for Rapid Frequency-Domain Aeroelastic Analysis", ,AIAA Paper 2011-3364, 2011.

[6] J.E. Carter, "A New Boundary-Layer Inviscid Iteration Technique for Separated Flow". AIAA Paper 1979-1450, July 1979.

[7] Bennett, R. M., Scott, R. C., and Wieseman, C. D., "Computational Test Cases for the Benchmark Active Controls Model", Journal of Guidance, Control, and Dynamics, Vol. 23, No. 5, September-October 2000.

[8] Rodden, W.P., Giesing, J.P. and Kalam, T.P., "New Method for Nonplanar Configurations," AGARD Conference Proceeding, CP-80-71, Pt, II, No. 4, 1971.

[9] Chen, P.C., Lee, H.W., and Liu, D.D., "Unsteady Subsonic Aerodynamics for Bodies and Wings with External Stores Including Wake Effect," Journal of Aircraft, Vol. 30, No. 5, Sep-Oct. 1933, p. 618-628.

[10] Bartels, R.E., and Schuster, D.M., "Comparison of Two Navier-Stokes Aeroelastic Methods Using BACT Benchmark Experimental Data," AIAA-99-3157-CP.

[11] Rivera, J.A., Dansberry B.E., Bennett, R.M., Durham, M.H., and Silva, W.A., "NACA 0012 Benchmark Model Experimental Flutter Results with Unsteady Pressure Distributions," AIAA-92-2396-CP.

[12] Chen, P.C., "A Damping Perturbation Methods for Flutter Solution: The g-Method," AIAA Journal, Vol. 38, No. 9, Sept. 2000.

10 COPYRIGHT STATEMENT